ACS APPLIED MATERIALS & INTERFACES

Research Article

www.acsami.org

In Situ Determination of the Pore Opening Point during Wet-Chemical Etching of the Barrier Layer of Porous Anodic Aluminum Oxide: Nonuniform Impurity Distribution in Anodic Oxide

Hee Han,[†,§] Sang-Joon Park,[‡,§] Jong Shik Jang,[†] Hyun Ryu,[†] Kyung Joong Kim,[†] Sunggi Baik,[‡] and Woo Lee*[,†]

[†]Korea Research Institute of Standards and Science (KRISS), Yuseong, Daejeon, 305-340, Korea

[‡]Department of Materials Science and Engineering, Pohang University of Science and Technology (POSTECH), Hyoja-dong, Pohang, 790-784, Korea

Supporting Information

ABSTRACT: Wet-chemical etching of the barrier oxide layer of anodic aluminum oxide (AAO) was systematically investigated by using scanning electron microscopy (SEM), secondary ion mass spectrometry (SIMS), and a newly devised experimental setup that allows accurate *in situ* determination of the pore opening point during chemical etching of the barrier oxide layer. We found that opening of the barrier oxide layer by wet-chemical etching can be significantly influenced by anodization time (t_{anodi}). According to secondary ion mass spectrometry (SIMS) analysis, porous anodic aluminum oxide (AAO) samples formed by long-term anodization contained a lower level of anionic impurity in the barrier oxide layer compared to the short-term anodized one and consequently exhibited retarded opening of the barrier oxide layer during the wet-chemical etching. The observed compositional dependence on the anodization time (t_{anodi}) in the barrier oxide layer is attributed to the progressive decrease of the electrolyte concentration upon anodization. The etching rate of the outer pore wall at the bottom part is lower than that of the one at the top part due to the lower level of impurity content in that region. This indicates that a concentration gradient of anionic impurity in the outer pore wall oxide may be established along both the vertical and radial directions of cylindrical pores. Apart from the effect of electrolyte concentration on the chemical composition of the barrier oxide layer, significantly decreased current density arising from the lowered concentration of electrolyte during the long-term anodization (~120 h) was found to cause disordering of pores. The results of the present work are expected to provide viable information not only for practical applications of nanoporous AAO in nanotechnology but also for thorough understanding of the self-organized formation of oxide nanopores during anodization.

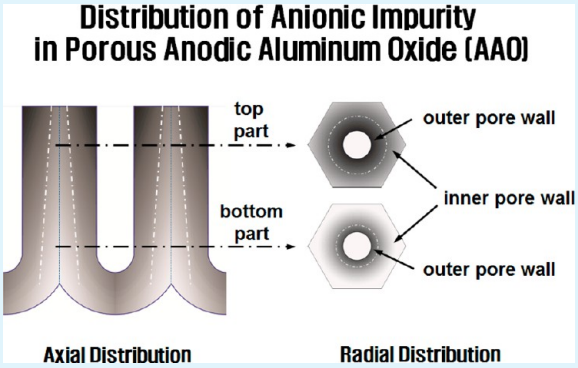

KEYWORDS: *anodic aluminum oxide, barrier layer etching, electrolyte concentration, chemical composition*

INTRODUCTION

Anodization is an electrochemical oxidation process of metals or semiconductors under either galvanostatic or potentiostatic conditions. Two types of anodic aluminum oxide (AAO) are formed depending on the electrolyte: one is a nonporous barrier-type oxide from a neutral electrolyte and the other is a porous-type oxide from an acidic electrolyte.[1−4] Technological interest has been focused particularly on the porous-type AAO due to the practical use for the fabrication of nanostructured materials[5−9] and the membranes for molecule separations.[10−13] Recently, substantial development of diverse anodization techniques such as hard anodization (HA),[14,15] pulse anodization (PA),[16−19] and cyclic anodization (CA)[20] has facilitated a tailoring of various structural parameters: pore size (D_p = 20−400 nm), interpore distance (D_{int} = 60−500 nm), pore density ($\rho = 10^8$−10^{10} cm^{-2}), channel length (hundreds of nanometers to hundreds of micrometers), and internal pore shape.

Figure 1 (part a) shows a schematic of the typical structure of porous-type AAO and (part b) the cross-section transmission electron microscope (TEM) image of the barrier oxide layer (BL). Cylindrical nanopores aligned perpendicular to the metal surface are self-ordered in the form of a close-packed hexagonal structure. The bottom of each nanopore is closed by a thin barrier oxide layer of hemispherical geometry. The pore wall of AAO has a bilayer structure in terms of chemical composition: relatively pure inner pore wall (light-gray in Figure 1a) and anion contaminated outer pore wall (dark-gray in Figure 1a).[4]

Received: February 7, 2013
Accepted: March 22, 2013
Published: March 22, 2013

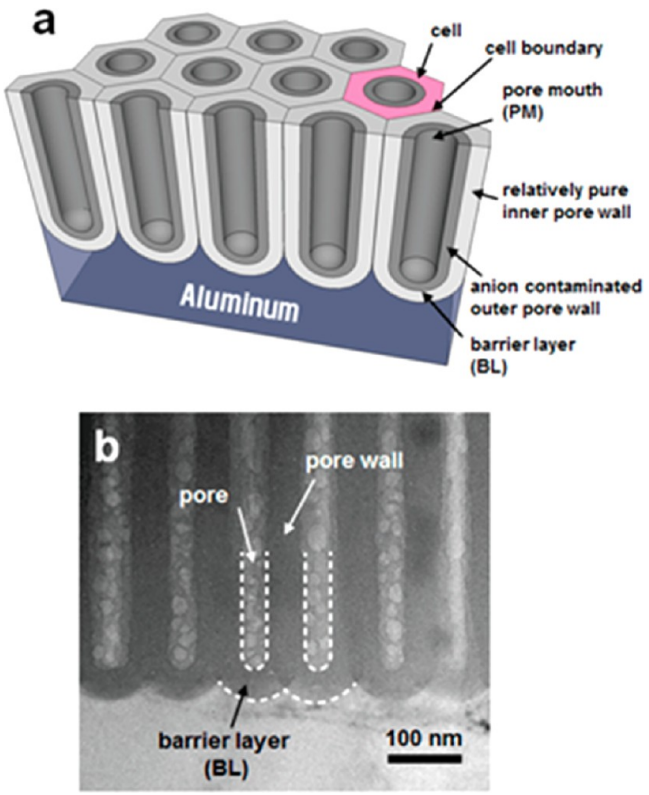

Figure 1. (a) Schematic showing an idealized structure of porous anodic aluminum oxide (AAO) with a self-organized array of hexagon cells and convex-shaped geometry of the barrier layer (BL) at the base of the pores. The two different regions of anion contaminated (dark gray) and relatively pure oxide (light gray) are also presented. (b) Cross-section TEM image of the bottom part of porous AAO.

For the most of practical uses of the porous AAO, removal of the barrier oxide layer is required. A lot of research has been intensively carried out in an attempt to develop an efficient way of opening the barrier oxide layer.[21−24] Dry etching processes employing an ion or neutral beam can provide precise control of the aperture size down to ∼10 nm at the barrier oxide layer. However, complicated processing steps requiring expensive equipment dilute the distinct advantages of the dry-etching methods. Wet-chemical etching, on the other hand, can be employed to remove the barrier oxide layer of a large area sample in a cheap and easy way. Despite the development of various techniques for the barrier oxide opening, there has been less attention to the oxide etching behavior depending on anodization conditions. In fact, the chemical composition of anodic oxide can be influenced by anodization conditions, such as type of electrolyte, voltage, current density (j), and etc.[4,16,25] It was reported that, for a given anodization voltage and electrolyte system, anodic oxide formed at high current density conditions (e.g., HA conditions) contains a higher level of anionic impurity compared to those formed at a lower current density one (e.g., MA conditions) and thus is labile against wet-chemical etching.[16]

In this article, we report the effect of electrolyte concentration on the barrier oxide etching behavior. The barrier oxide opening time was found to be increased with increasing the thickness of porous AAO, viz., anodization time (t_{anodi}). According to secondary ion mass spectrometry (SIMS) analysis, a lower level of anion impurity content (carbon-based species in the present work) was incorporated into the barrier oxide layer of AAO formed by long-term anodization, compared to those formed by short-term anodization. We attribute the observed compositional change of the barrier oxide layer to the decreased electrolyte concentration during the anodization process. The etching rate of the outer pore wall at the top part of porous AAO was found to be higher, compared to that at the bottom part of AAO, indicating the gradual variation of anionic impurity content (i.e., establishment of gradient of impurity concentration) along the pore growth direction. Besides the change of oxide composition caused by progressively decreasing the electrolyte concentration, it was also observed that disordering of pores occurs due to the decreased current density (j) during long-term anodization. On the basis of our experimental results, it is suggested that barrier oxide layer etching process should be carefully controlled depending on the anodization conditions for making the use of porous AAO more reliable and reproducible.

EXPERIMENTAL SECTION

Preparation of Porous Anodic Aluminum Oxide (AAO). As-received Al discs (Goodfellow, 99.999%, typical diameter = 2 cm) were electropolished in a vigorously stirred mixture solution of 65% $HClO_4$ and 95% ethanol (1:3−1:4 in volume ratio) to rule out the effect of locally enhanced anodization coming from the surface roughness. Self-ordered AAO was prepared by two-step anodization of the electropolished Al disc. The first anodization was performed by using 0.3 M $H_2C_2O_4$ (7 °C) as an electrolyte at 40 V for 24 h. The resulting AAO layer was completely removed by immersing the sample in a mixture solution of 1.8 wt % H_2CrO_4 and 6 wt % H_3PO_4 at 45 °C for more than 12 h to remove the oxide layer with a disordered pore structure. Next, the resulting Al substrate with highly ordered arrays of approximately hemispherical concaves was anodized under the same conditions as the first anodization. Each concavity on the surface of the Al substrate serves as a pore initiation site during the second anodization. In the present work, the duration of the second anodization was varied from 0.5 to 24 h in order to investigate the effect of anodization time (t_{anodi}) on the wet-etching behavior of the barrier oxide layer. After anodization, Al substrate was removed by using an aqueous mixture solution containing 3.4 g of $CuCl_2{\cdot}2H_2O$, 50 mL of 38 wt % HCl, and 100 mL of deionized water (DI water) in order to expose the surface of the barrier oxide layer.

***In Situ* Detection of Opening of Barrier Layer (BL).** For accurate *in situ* determination of the pore opening point during wet-chemical etching of the barrier oxide layer, we devised an H-cell consisting of two Teflon half cells (see the inset of Figure 3 and Figure S1 in the Supporting Information). As-prepared AAO was sandwiched between the two half-cells by using a pair of O-rings (i.d. = 8 mm). After that, the half-cell that faces the bottom surface (i.e., BL side) of the porous AAO was filled with 5 wt % H_3PO_4 for wet-chemical etching of the barrier oxide layer, while the other half-cell was filled with DI water. The assembled H-cell was immersed in a thermostatted water-bath (29.0 ± 0.2 °C). A pair of Pt electrodes (wire thickness = 0.5 mm) was placed just in front of the top surface of porous AAO (i.e., pore mouth, PM, side), which was in contact with DI water. Current between two Pt electrodes was monitored by using a two-channel source-measure unit (Keithley 2612A) under a voltage bias of 2 V. Previously, Lillo and Losic immersed two Pt electrodes into the respective

half-cells (i.e., across the porous AAO) to monitor the current signal during the etching process and continuously stirred solutions by using a magnetic stirrer (ref 22). We found, however, that such an electrode configuration can affect the opening of the barrier oxide layer due to field-assisted dissolution of the barrier oxide by the etchant solution. Apart from the electrode configuration, we also found that mechanical agitation of the etchant solution can influence the barrier oxide etching; the faster the stirring of the solution, the faster the opening of the barrier oxide layer. Therefore, we carried out all of our experiments without stirring of the solutions. During wet-chemical etching, temperature stability of the experimental setup was monitored by using a 24-bit universal analog input module (National Instrument, NI9219) with a Pt-resistance temperature detector (Pt-RTD) immersed in the etchant solution.

Determination of Pore Wall Etching Rate. Porous AAO sample was cut into several pieces to prepare two different kinds of specimens, AAOs with and without a residual Al layer for oxide etching at the top and bottom part of AAO, respectively. The Al layer was removed by dipping the samples into the aqueous mixture solution containing 3.4 g of $CuCl_2 \cdot 2H_2O$, 50 mL of 38 wt % HCl, and 100 mL of DI water. The pore mouth surface of the resulting free-standing AAO was tightly glued on the Si substrates, so that the undesired wet-chemical etching of the barrier layer from the base of pores can be completely prevented. After that, the samples were immersed into 5 wt % H_3PO_4 solution (29 °C) for various etching times (t_{etch}) for the investigation of the etching behavior of both the top and bottom parts of the AAO.

Microscopic Characterization. A Hitachi S-4800 field emission scanning electron microscope (FE-SEM) was used to characterize the morphology of the samples. The transmission electron microscope (TEM, Tecnai G^2, FEI) operated at a primary beam energy of 300 kV with a resolution of 2.0 nm was employed to characterize the cross-sectional morphology of the barrier oxide layer. The samples for TEM investigations were prepared by the standard method. An as-prepared free-standing AAO was glued on a piece of silicon substrate by using an epoxy resin, then mechanically polished to a thickness of about 100 μm, dimpled from one side to get a thickness of about 20 μm at the center, and followed by argon ion milling under an acceleration voltage of 3 kV by using a Gatan precision ion polishing system.

Characterization of Chemical Composition of Barrier Oxide Layer. The amount of carbon incorporated into the barrier oxide layer in the form of anionic impurity was analyzed through secondary ion mass spectrometry (SIMS, Cameca IMS-7f, France) depth profiling with a Cs^+ ion beam of 6 keV.

RESULTS AND DISCUSSION

In a typical anodization of aluminum, the thickness of the resulting AAO (i.e., the length of nanopores) is linearly proportional to the total amount of charge involved in the electrochemical oxidation reaction (i.e., anodization time, t_{anodi}, Figure S2 in the Supporting Information). For our anodization condition, the growth rate of AAO turned out to be 3.44 μm/h.

The representative SEM images in Figure 2 shows the evolution of the bottom surface morphologies upon wet-chemical etching of AAOs formed by anodization for different periods of time (t_{anodi}) ranging from 0.5 to 24 h. Upon 30 min of etching, the barrier layer of AAOs prepared by 0.5 h- and 8 h-anodization were opened (see the first column of Figure 2).

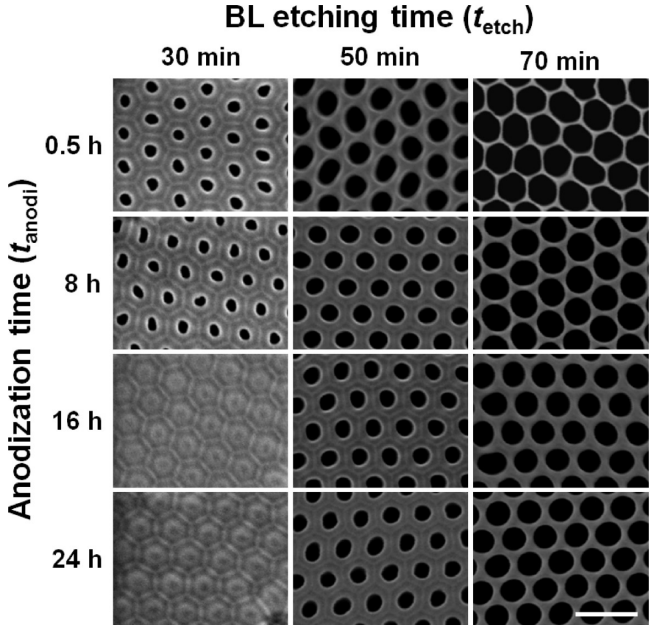

Figure 2. Field emission scanning electron microscopy (FE-SEM) images of the bottom surface of porous AAOs, showing the anodization time (t_{anodi}) dependence of opening of the barrier oxide layers (BL) upon wet-chemical etching in 5 wt % H_3PO_4 at 29 ± 0.2 °C. Scale bar is 200 nm.

On the other hand, opening of the barrier layer did not take place in the case of AAO samples formed by a longer period of time (i.e., t_{anodi} > 16 h). This experimental observation clearly indicates that the opening of the barrier oxide layer is influenced by anodization time (t_{anodi}), that is the thickness of AAO. After opening of the barrier layer, the size of the pores was systematically increased due to the etching of pore-wall oxide by the etchant solution, which will be discussed later in detail (Figure 8, *vide infra*). For the same period of etching time (t_{etch}), pores of AAO formed by short-term anodization appeared to be widened to a larger extent, compared to those of long-term anodized samples (see the second and third columns of Figure 2).

In order to determine the accurate onset of barrier oxide layer opening depending on the anodization time (t_{anodi}), we devised an *in situ* method of pore opening detection, by improving the experimental setup employed by Lillo and Losic (see the Experimental Section).[22] Figure 3 shows current−time curves measured during the wet-chemical etching of barrier oxide layer of porous AAO samples prepared by anodization of aluminum for different periods of time (t_{anodi} = 1, 8, 16, and 24 h). The curves are characterized (1) by a small and steady current flow at the early stage of etching, of which the amount is determined by the conductivity of DI water, (2) by an abrupt increase at the onset of the barrier layer opening due to the influx of an acidic etchant solution (i.e., H_3PO_4) toward the half-cell containing DI water through the opened nanopores, and (3) by fluctuation of current after passing through an overshoot due to convective flow of etchant solution across through-hole AAO membrane under unstirred solution conditions. As evident from the curves, opening of the barrier layer exhibited clear dependence on the anodization time (t_{anodi}) from t_{etch} = 30 min for 1 h-anodized AAO (i.e., t_{anodi} = 1 h) to t_{etch} = 43 min for 24 h-anodized AAO (i.e., t_{anodi} = 24 h),

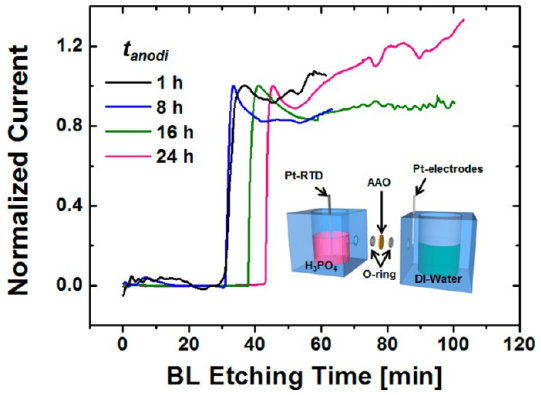

Figure 3. Current−time transient during wet-chemical etching of the barrier layer of porous AAO fabricated by 1 h- (black), 8 h- (blue), 16 h- (green), and 24 h-anodization (pink). The inset shows a schematic of the experimental setup used for detecting the barrier layer opening point.

although the dependence is rather weak for short-term anodized samples (i.e., t_{anodi} = 1 and 8 h).

It is assumed that the reasons responsible for the marked difference in the pore opening time would be either the different thicknesses or chemical composition of the barrier oxide. According to the high field conduction theory,[26] the barrier layer thickness (t_b) is inversely proportional to the logarithm of the current density (j):

$$j = j_0 \exp(\beta E) = j_0 \exp(\beta \Delta U / t_b) \quad (1)$$

where j_0 and β are the material-related constants, E is the effective electric field strength ($\Delta U/t_b$), and t_b is the barrier layer thickness. In our typical long-term anodization experiments, current density (j) was observed to be decreased about 0.2 mA/cm^2 over t_{anodi} = 24 h, which would cause only about 0.025% (equivalent to 0.1 Å) increase of the barrier layer thickness (t_b). From TEM investigation, it was also confirmed that the thicknesses of 1 h- and 24 h-anodized AAOs were almost the same (i.e., ∼40 nm, see Figure S3 in the Supporting Information). Therefore, we may ignore the contribution of the thickness increase of the barrier layer to the retarded opening of the pores. All the experimental conditions were kept constant during the anodization process except t_{anodi}. One may assume that a change in pH or conductivity of the electrolyte used for different anodization time (t_{anodi}) affects the chemical properties of the barrier oxide. In fact, we found that pH does not show a meaningful change, but only the conductivity of electrolyte gradually increases with t_{anodi}, possibly due to the increased amount of Al^{3+} cations during anodization (see Figure S4 in the Supporting Information). It has been reported that the pH of the electrolyte may affect the pore size or pore ordering of AAO.[26] However, to the best of our knowledge, there have been no reports on the change of pH upon t_{anodi} or on the pH dependence of the chemical composition of anodic oxide. Thus we believed that the only reason for the difference in the barrier oxide layer opening onset is the change in the chemical composition of the barrier oxide (i.e., material-related constant, β in eq 1) due possibly either to the reduced concentration of the electrolyte (i.e., $H_2C_2O_4$) or to the large concentration gradient of the electrolyte established along the extended nanochannels in the case of long-term anodization.

We further investigated the barrier oxide layer etching behavior by using porous AAO fabricated by anodization for 23 h followed by an additional 1 h of anodization (total t_{anodi} = 24 h) by using fresh 0.3 M $H_2C_2O_4$ solution (see Figure S5 in the Supporting Information). The barrier oxide layer was observed to be opened at a much shorter time (t_{etch} ∼30 min) than that of 24 h-anodized AAO (t_{etch} ∼43 min) despite the same total anodizaiton time (i.e., t_{anodi} = 24 h). This result indicates clearly that the pore opening time is highly correlated with the concentration of bulk anodization electrolyte, ruling out the effect of the concentration gradient established along the long nanochannels.

Since current in anodization is related to the mass transport of oxygen-containing anions from the electrolyte to the oxide/metal interface through the barrier oxide layer,[27] a progressive decrease of current during anodization over an extended period of time implies a decrease of the amount of anionic impurities ($C_2O_4^{2-}$ in the present study) incorporated into the barrier oxide (see Figure S6 in the Supporting Information). In other words, the concentration gradient of the anionic impurity in the pore wall oxide exists along the pore growth direction. In general, anodic oxide containing a larger amount of anionic impurity is highly labile against wet-chemical etching due to the less dense nature.[16] Accordingly, the time required for opening of the barrier oxide layer upon wet-chemical etching decreases with a decrease in the anodization time (t_{anodi}).

For the investigation of the compositional change of the barrier oxide layer with t_{anodi}, secondary ion mass spectrometry (SIMS) depth profiling was performed on the barrier oxide layers of porous AAO fabricated by anodization for different periods of time (t_{anodi}). Figure 4 shows relative intensities of Al (blue), C (red), and O (black) obtained from 1 h-anodized (upper panel) and 24 h-anodized porous AAO (lower panel), and the amount of C incorporated into the barrier oxide was

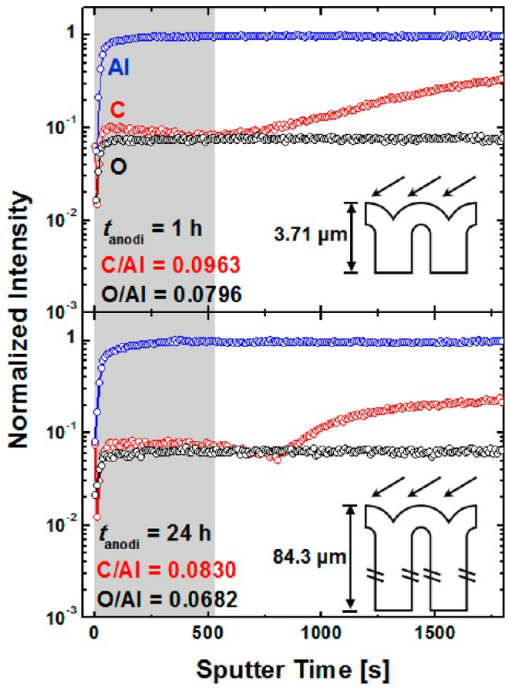

Figure 4. SIMS depth profiles of the bottom sides of porous AAOs fabricated by 1 h- (upper) and 24 h-anodization (lower). Al, O, and C elements are indicated as blue, black, and red symbols, respectively. The insets are schematic cross-sections of the respective samples. Arrows in the insets indicate an incident ion beam. The gray-shaded regions (i.e., below 530 s) were considered for compositional analysis.

dx.doi.org/10.1021/am400520d | ACS Appl. Mater. Interfaces 2013, 5, 3441−3448

qualitatively analyzed with a relative ratio of the SIMS intensities. The insets of the upper and lower panels are schematic cross sections of porous AAOs with different thicknesses. To prevent the brittle AAOs from breaking during the specimen preparation for SIMS measurements, the pore mouth side of AAO was coated with nail-polish, which contributed to the increase of the C intensity when barrier oxide layer was opened by a sputtered ion beam during SIMS measurement. For this reason, SIMS profiles below 530 s (i.e., shaded region of the graphs) were considered in compositional analysis. From the relative ratio of intensities of C to Al, it was found that the relative amount of C in the barrier oxide layer is about 13.8% higher for 1 h-anodized AAO than that of 24 h-anodized AAO. This analytical result manifests from the AAOs formed by short-term anodization are contaminated by an anionic impurity to a larger extent, compared to the long-term counterparts.

The effect of electrolyte concentration on the barrier oxide layer etching could be further explored by performing a set of etching experiments with porous AAOs formed in $H_2C_2O_4$ solutions of different concentrations. We carried out additional anodizations at 40 V on the 24 h-preanodized AAO samples by using fresh $H_2C_2O_4$ solutions of two different concentrations, i.e., 0.03 and 0.3 M. In order to ensure the same thickness of the newly formed anodic oxide by the additional anodization, we employed a charge controlled anodization technique, in which the anodization was terminated when the total integrated charge reached 1.5 C/cm^2 (see Figure S7 in the Supporting Information). Figure 5 shows the current−time transients

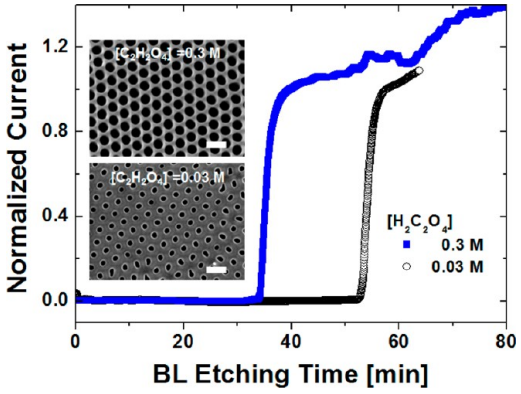

Figure 5. Current−time curves obtained during wet-chemical etching of the barrier oxide layers of AAOs formed in 0.3 M (blue filled square) and 0.03 M $H_2C_2O_4$ (black open circle). The insets show typical SEM images of the bottom surface of the respective AAO samples after removal of the barrier oxide layer by wet-chemical etching for t_{etch} = 55 min. Scale bars are 200 nm.

obtained during the barrier layer etching of the samples. In the case of AAO prepared by using fresh 0.3 M $H_2C_2O_4$, opening of the barrier layer started at 33 min, which is almost the same as that of the 0.5 h-anodized sample (t_{etch} = 30 min) in Figure 2. On the other hand, AAO fabricated by 0.03 M $H_2C_2O_4$ exhibited a significantly retarded opening of the barrier layer (t_{etch} = 53 min), which is even longer than that (t_{etch} = 43 min) of the 24 h-anodized sample.

Figure 6 shows SIMS depth profiles of the corresponding samples. It is clear from the figure that the amount of C for the sample fabricated using 0.3 M $H_2C_2O_4$ was 2.17 times higher than that for one fabricated using 0.03 M $H_2C_2O_4$, indicating

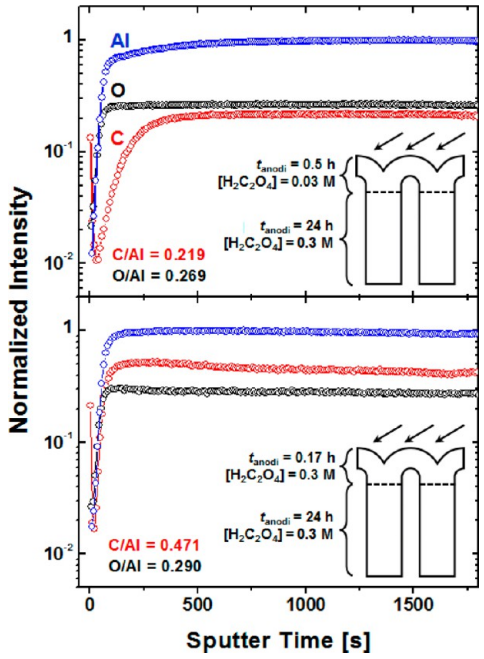

Figure 6. SIMS depth profiles of the bottom sides of AAOs prepared by using 0.03 M (upper) and 0.3 M $H_2C_2O_4$ (lower). Concentration profiles of Al, O, and C are presented as blue, black, and red symbols, respectively. The insets are schematic cross-sections of the respective samples. Arrows in the insets indicate an incident ion beam.

that a larger amount of anionic impurities from anodizing electrolyte was incorporated into the barrier oxide of the former, thus resulting in the poor chemical stability against the etchant. This observation undoubtedly confirms again that the anodization time (t_{anodi}) dependence of the barrier opening time (as shown in Figure 2) is the consequence of the decrease of the electrolyte concentration upon anodization for an extended period of time.

The morphological change of the bottom surface of AAO with etching time (t_{etch}) was investigated in more detail by SEM investigation, which would provide useful information for the practical use of porous AAO (Figure 7). Porous AAO samples were prepared by performing anodization for 24 h at 40 V using 0.3 M $H_2C_2O_4$. Opening of the barrier layer was carried out by using 5 wt % H_3PO_4 (29 °C) as an etchant. As depicted in the SEM micrographs, the bottom surface of as-prepared AAO (i.e., t_{etch} = 0 min sample in Figure 7) is characterized by hexagonally close-packed arrays of hemispherical domes. Consistently with the results reported in ref 21, barrier oxide was gradually etched from the entire surface of each dome, exposing the relatively pure hexagonal cell boundaries. The pore bottom of AAO was still closed at t_{etch} = 40 min, which is in line with the results shown in Figures 1 and 2. Opening of the barrier layer occurs at the very center of the hemispherical dome. The barrier oxide layer was completely removed upon t_{etch} = 50 min of the wet-chemical etching, accompanied with pore widening.

Figure 8 shows the increase of pore diameter (D_p) of the pores at the top (filled circle) and bottom (open circle) part of the 24 h-anodized porous AAO upon wet-chemical etching. For the determination of the mean diameters of the pores, SEM micrographs obtained from the bottom (Figure 7) and top parts (Figure S8 in the Supporting Information) of the AAO membranes were processed by using standard image processing software (i.e., Image *J*).[28] Pore diameter (D_p) of the top and

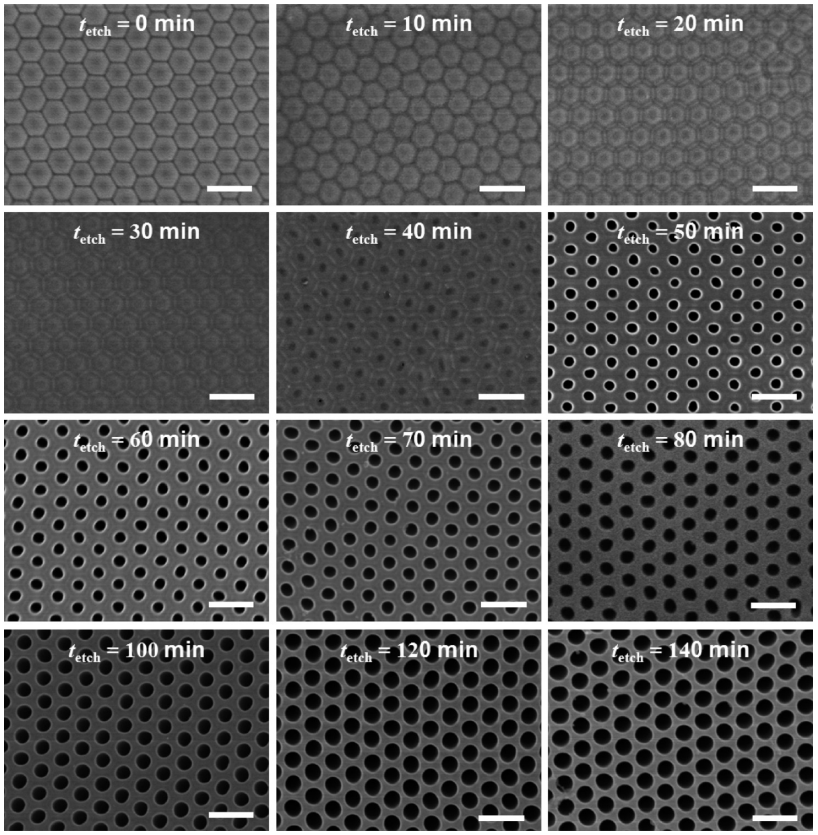

Figure 7. SEM micrographs showing the morphological evolution of the bottom surface of AAO depending on different etching times (t_{etch}) in 5 wt % H_3PO_4 at 29 ± 0.2 °C. Scale bars are 200 nm.

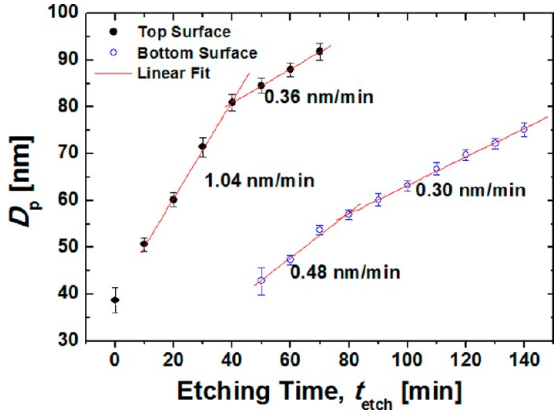

Figure 8. Variation of pore diameter (D_p) at the top (filled circles) and bottom (open circle) part of the AAO membranes with their linear fits as a function of etching time (t_{etch}).

bottom parts of the AAO membrane increased linearly with etching time (t_{etch}). As manifested in the Figure 8, the curves can be characterized with two characteristic regions depending on the pore wall etching rate; one is the fast etching region stemming from the etching of the anion-contaminated outer pore wall of AAO and the other is the slow etching region originating from the etching of the relatively pure inner pore wall. It is worth noting that the etching rate of the outer pore wall at the top part of the AAO (1.04 nm/min) is higher than that at the bottom part (0.48 nm/min), whereas almost the same etching rate for the inner pore wall (0.36 and 0.30 nm/min for the top and bottom parts, respectively). This result can be also ascribed to the lowered impurity contents in the outer pore wall oxide at the bottom part of the AAO as a result of a progressive decrease in electrolyte. In order to verify the difference in the amount of anionic impurity content at the top and bottom parts of the AAO, SIMS analysis was carried out (see Figure S9 in the Supporting Information). The amount of C at the top part was observed to be about 3 times higher than that at bottom part. Upon closer inspection of the present results, we could deduce that the outer pore wall at the top part of AAO is about 2.3 times thicker than that at the bottom part: the thickness of the outer pore wall at the top and bottom parts of AAO is estimated to be 67.7% and 29.0% of the thickness of the pore wall, respectively. This implies that the thickness ratio of the relatively pure inner pore wall to the anion-contaminated outer pore wall is gradually varied along the pore axis during anodization of aluminum (see Figure S10 in the Supporting Information). It was reported that anodization current is closely correlated with the relative extents of the inner and outer pore walls in the anodic oxide.[4] Thus, the observed variation of the thickness of the outer pore wall would be ascribed to the decrease of current density (j) due to the decreased electrolyte concentration.

Anodic oxidation of aluminum is a volume expansion process, causing mechanical stress at the metal/oxide interface. The resulting mechanical stress has been regarded as a driving force for the self-organized formation of oxide nanopore during steady-state anodization of aluminum.[29] On the other hand, the degree of impurity incorporation into anodic oxide is positively correlated with the volume expansion during anodic oxidation of aluminum, in a way that the inverse volume expansion factor is linearly dependent on the logarithm of the current density

(j).[30] Accordingly, for a given anodization condition, it is expected that the degree of pore ordering increases with the level of anion incorporation (i.e., mechanical stress); the more the impurity incorporation into anodic oxide, the higher the degree of pore ordering due to a higher level of repulsive stress between pores. In fact, we found that anodization for over a certain period of time (e.g., t_{anodi} = 120 h) results in disordering of pores (see Figure S11 in the Supporting Information) due to a decreased level of anionic impurity that is associated with decreased electrolyte concentration. For thorough understanding on the steady-state growth of anodic oxide, we are currently performing a systematic investigation on the effect of anodization time (t_{anodi}) and electrolyte concentration on the ordering of nanopores. The results will be reported elsewhere. Incorporation of anionic impurity also has profound implication to the steady-state growth of porous alumina. Recent experimental and theoretical studies suggested that incorporated anionic species play an important role in the viscous flow of oxide materials from the pore base toward the cell boundary region.[31,32] Therefore, our finding on nonuniform distribution of anionic impurity may provide important information for thorough understanding of steady-state growth of self-organized nanopores during anodization of aluminum.

CONCLUSION

The effect of anodization time (t_{anodi}) and electrolyte concentration on the chemical composition and thus wet-chemical etching behavior of the barrier oxide layer of AAO was systematically investigated by using SEM, SIMS, and a newly devised experimental setup that allows accurate *in situ* determination of the pore opening point during wet-chemical etching of the barrier oxide layer. AAO samples formed by long-term anodization exhibited significantly retarded opening of the barrier oxide layer compared to the short-term anodized samples due to the lower level of anionic impurity incorporated into the anodic oxide during anodization. On the basis of our control anodization experiments and SIMS analysis on the resulting AAO samples, the observed compositional dependence of the barrier oxide on the anodization time (t_{anodi}) was attributed to the progressive decrease of the electrolyte concentration during anodization. Our extensive pore widening experiments indicated that the decrease of the electrolyte concentration also causes a decrease of the relative thickness of the anion contaminated outer pore wall to the pure inner pore wall. All of our results revealed the presence of the nonuniform distribution of impurity in AAO along both the vertical and radial direction of cylindrical nanopores, as schematically illustrated in Figure 9. We found that electrolyte concentration plays an important role in ordering of pores, especially during long-term anodization of aluminum. Our results are expected to provide viable information not only for practical applications of nanoporous AAO in nanotechnology but also for thorough understanding of the self-organized formation of oxide nanopores during anodization.

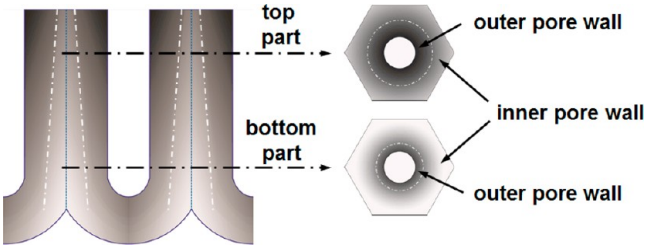

Figure 9. Schematics illustrating the nonuniform distribution of anionic impurity in porous AAO. A different level of impurity in anodic oxide is depicted with gray scale. White dashed lines correspond to the interface between the anion contaminated outer pore wall and the relatively pure inner pore wall.

ASSOCIATED CONTENT

Supporting Information

A Photograph of H-cell, thickness of AAO and the corresponding total charge as a function of t_{anodi}, cross-section TEM images of 1 and 24 h-anodized AAO, conductivity and pH of electrolyte as a function of t_{anodi}, current-time transient during the etching of the barrier layer of AAO anodized for 23 h followed by additional 1 h-anodization using fresh electrolyte, current-time transient obtained during the second anodization of Al, current-time and charge-time curves obtained during the additional anodization of second-anodized AAOs prepared by using 0.3 M and 0.03 M $H_2C_2O_4$, SEM images of AAO after etching of pore wall for different tetch, SIMS depth profile of top and bottom part of 72 h-anodized AAOs, a schematic of AAO illustrating non-uniform distribution of anionic impurity along the pore axes, and SEM images of bottom surface of 24, 48, 72, and 120 h-anodized AAOs. This material is available free of charge via the Internet at http://pubs.acs.org.

AUTHOR INFORMATION

Corresponding Author

*E-mail: woolee@kriss.re.kr.

Author Contributions

§H.H. and S.-J.P. contributed equally.

Notes

The authors declare no competing financial interest.

ACKNOWLEDGMENTS

This work was supported by Future-Based Technology Development Program (Nano Fields) through the National Research Foundation of Korea (NRF) funded by the Ministry of Education, Science and Technology (Grant No. 20120009623).

REFERENCES

(1) Diggle, J. W.; Downie, T. C.; Goulding, C. W. *Chem. Rev.* **1969**, *69*, 365−405.
(2) Keller, F.; Hunter, M. S.; Robinson, D. L. *J. Electrochem. Soc.* **1953**, *100*, 411−419.
(3) Hunter, M. S.; Fowle, P. *J. Electrochem. Soc.* **1954**, *101*, 481−485.
(4) Thompson, G. E.; Wood, G. C. *Nature* **1981**, *290*, 230−232.
(5) Lee, W.; Han, H.; Lotnyk, A.; Schubert, M. A.; Senz, S.; Alexe, M.; Hesse, D.; Baik, S.; Gösele, U. *Nat. Nanotechnol.* **2008**, *3*, 402−407.
(6) Huang, Z.; Zhang, X.; Reiche, M.; Liu, L.; Lee, W.; Shimizu, T.; Senz, S.; Gösele, U. *Nano Lett.* **2008**, *8*, 3046−3051.
(7) Liu, K.; Fournier-Bidoz, S.; Ozin, G. A.; Manners, I. *Chem. Mater.* **2009**, *21*, 1781−1783.
(8) Liu, L.; Lee, W.; Scholz, R.; Pippel, E.; Gösele, U. *Angew. Chem., Int. Ed.* **2008**, *47*, 7004−7008.
(9) Zhang, D.; Luo, L.; Liao, Q.; Wang, H.; Fu, H.; Yao, J. *J. Phys. Chem. C* **2011**, *115*, 2360−2365.
(10) Jun, I.-K.; Hess, H. *Adv. Mater.* **2010**, *22*, 4823−4825.
(11) Jani, A. M. M.; Anglin, E. J.; McInnes, S. J. P.; Losic, D.; Shapter, J. G.; Voelcker, N. H. *Chem. Commun.* **2009**, 3062−3064.

(12) Ingham, C. J.; ter Maat, J.; de Vos, W. M. *Biotechnol. Adv.* **2012**, *30*, 1089−1099.
(13) Jani, A. M. M.; Kempson, I. M.; Losic, D.; Voelcker, N. H. *Angew. Chem., Int. Ed.* **2010**, *49*, 7933−7937.
(14) Lee, W.; Ji, R.; Gösele, U.; Nielsch, K. *Nat. Mater.* **2006**, *5*, 741−747.
(15) Schwirn, K.; Lee, W.; Hillebrand, R.; Steinhart, M.; Nielsch, K.; Gösele, U. *ACS Nano* **2008**, *2*, 302−310.
(16) Lee, W.; Schwirn, K.; Steinhart, M.; Pippel, E.; Scholz, R.; Gösele, U. *Nat. Nanotechnol.* **2008**, *3*, 234−239.
(17) Lee, W.; Scholz, R.; Gösele, U. *Nano Lett.* **2008**, *8*, 2155−2160.
(18) Lee, W.; Kim, J.-C. *Nanotechnol.* **2010**, *21*, 485304.
(19) Losic, D.; Lillo, M.; Losic, D., Jr. *Small* **2009**, *5*, 1392−1397.
(20) Han, C. Y.; Willing, G. A.; Xiao, Z.; Wang, H. H. *Langmuir* **2007**, *23*, 1564−1568.
(21) Lillo, M.; Losic, D. *J. Membr. Sci.* **2009**, *327*, 11−17.
(22) Yeon, J. K.; Lim, W. S.; Park, J. B.; Kwon, N. Y.; Kim, S. I.; Min, K. S.; Chung, I. S.; Kim, Y. W.; Yeom, G. Y. *J. Electrochem. Soc.* **2011**, *158*, D254−D258.
(23) Xu, T.; Zangari, G.; Metzger, R. M. *Nano Lett.* **2002**, *2*, 37−41.
(24) Vrublevsky, I.; Parkoun, V.; Sokol, V.; Schreckenbach, J. *Appl. Surf. Sci.* **2004**, *236*, 270−277.
(25) Lohrengel, M. M. *Mater. Sci. Eng.: R* **1993**, *11*, 243−294.
(26) Nielsch, K.; Choi, J.; Schwirn, K.; Wehrspohn, R. B.; Gösele, U. *Nano Lett.* **2002**, *2*, 677−680.
(27) Parkhutik, V. P.; Shershulsky, V. I. *J. Phys. D: Appl. Phys.* **1992**, *25*, 1258−1263.
(28) Rasband, W. *Image J*, release 1.36b; NIH: Bethesda, MD, 2006; http://rsb.info.nih.gov/ij/.
(29) Jessensky, O.; Müller, F.; Gösele, U. *Appl. Phys. Lett.* **1998**, *72*, 1173−1175.
(30) Vrublevsky, I.; Parkoun, V.; Schreckenbach, J.; Marx, G. *Appl. Surf. Sci.* **2003**, *220*, 51−59.
(31) Garcia-Vergara, S. J.; Skeldon, P.; Thompson, G. E.; Habazaki, H. *Electrochim. Acta* **2006**, *52*, 681−687.
(32) Houser, J. E.; Hebert, K. R. *Nat. Mater.* **2009**, *8*, 415−420.